

# Ligand-Stabilized and Atomically Precise Gold Nanocluster Catalysis: A Case Study for Correlating Fundamental Electronic Properties with Catalysis

Jing Liu,<sup>[a, b]</sup> Katla Sai Krishna,<sup>[a, b]</sup> Yaroslav B. Losovyj,<sup>[a, b]</sup> Soma Chattopadhyay,<sup>[c]</sup> Natalia Lozova,<sup>[a]</sup> Jeffrey T. Miller,<sup>[d]</sup> James J. Spivey,<sup>[b]</sup> and Challa S. S. R. Kumar<sup>\*,[a, b]</sup>

**Abstract:** We present results from our investigations into correlating the styrene-oxidation catalysis of atomically precise mixed-ligand biicosahedral-structure  $[\text{Au}_{25}(\text{PPh}_3)_{10}(\text{SC}_{12}\text{H}_{25})_5\text{Cl}_2]^{2+}$  ( $\text{Au}_{25}\text{-bi}$ ) and thiol-stabilized icosahedral core-shell-structure  $[\text{Au}_{25}(\text{SCH}_2\text{CH}_2\text{Ph})_{18}]^-$  ( $\text{Au}_{25}\text{-i}$ ) clusters with their electronic and atomic structure by using a combination of synchrotron radiation-based X-ray absorption fine-structure spectroscopy (XAFS) and ultraviolet photoemission spectroscopy (UPS). Compared to bulk Au, XAFS revealed low Au–Au coordination, Au–

Au bond contraction and higher d-band vacancies in both the ligand-stabilized Au clusters. The ligands were found not only to act as colloidal stabilizers, but also as d-band electron acceptor for Au atoms.  $\text{Au}_{25}\text{-bi}$  clusters have a higher first-shell Au coordination number than  $\text{Au}_{25}\text{-i}$ , whereas  $\text{Au}_{25}\text{-bi}$  and  $\text{Au}_{25}\text{-i}$  clusters have the same

number of Au atoms. The UPS revealed a trend of narrower d-band width, with apparent d-band spin–orbit splitting and higher binding energy of d-band center position for  $\text{Au}_{25}\text{-bi}$  and  $\text{Au}_{25}\text{-i}$ . We propose that the differences in their d-band unoccupied state population are likely to be responsible for differences in their catalytic activity and selectivity. The findings reported herein help to understand the catalysis of atomically precise ligand-stabilized metal clusters by correlating their atomic or electronic properties with catalytic activity.

**Keywords:** cluster compounds • gold • nanostructures • ultraviolet photoemission spectra • X-ray absorption fine structure

## Introduction

Colloidal nanoparticle catalysts continue to attract attention both for solution<sup>[1]</sup> and for gas-phase catalysis.<sup>[2,3]</sup> The influence of their size, shape, and oxidation state on their catalysis was previously investigated.<sup>[4–7]</sup> Their catalytic activity and selectivity are generally known to increase when the cluster size decreases to about 1 nm or below.<sup>[8]</sup> Of the nano-

particle catalysts, there has been significant work on gold nanoparticles, especially as catalysts for liquid–solid and gas–solid oxidation reactions.<sup>[9,10]</sup> Their size- and shape-dependent catalytic properties have also been examined.<sup>[11–15]</sup> For instance, Goodman and co-workers have reported an unusual size-dependent catalytic behavior of chemical-vapor-deposited gold clusters (1–6 nm) on single-crystalline titania surface for CO oxidation.<sup>[16]</sup> Theoretical studies by Landman and co-workers<sup>[17]</sup> have shown that the  $\text{Au}_8$  is the smallest catalytically active size for the CO oxidation. Several attempts have been made to investigate their structure–catalytic-activity relationships.<sup>[18]</sup> However, there have been very few attempts to directly correlate their fundamental electronic structure with their catalytic properties.<sup>[19–21]</sup> One of the main reasons for this is the polydispersity issue of gold nanoparticles. With recent successes in the synthesis of atomically precise ultra-small gold-cluster catalysts, there is now an opportunity to obtain new knowledge about their electronic structure–catalytic-activity relationships.<sup>[12,22–24]</sup>

There are a number of experimental and computational studies on the catalytic activity of atomically precise gold clusters.<sup>[2,24–28]</sup> The CO oxidation was explored by Spivey and co-workers<sup>[2]</sup> for ligand-stabilized atomically precise  $\text{Au}_{38}$  clusters supported on titania. Their results showed that supported Au clusters of controllable size can be prepared by thiol-ligated solution-based method. Recently, Jin and co-workers<sup>[24]</sup> have studied and compared the catalytic activity of silica-supported gold clusters  $\text{Au}_{25}$ ,  $\text{Au}_{38}$ , and  $\text{Au}_{144}$  for styrene oxidation by using both dioxygen and *tert*-butyl hy-

[a] Dr. J. Liu, Dr. K. S. Krishna, Dr. Y. B. Losovyj, Dr. N. Lozova, Dr. C. S. S. R. Kumar

Center for Advanced Microstructures and Devices (CAMD)  
Louisiana State University, Baton Rouge, LA 70806 (USA)

[b] Dr. J. Liu, Dr. K. S. Krishna, Dr. Y. B. Losovyj, Prof. J. J. Spivey, Dr. C. S. S. R. Kumar

Center for Atomic-Level Catalyst Design  
324, Cain Department of Chemical Engineering  
Louisiana State University, 110 Chemical Engineering  
South Stadium Road, Baton Rouge, LA 70803 (USA)  
E-mail: ckumar1@lsu.edu

[c] Dr. S. Chattopadhyay  
CSRRI-IIT, MRCAT, Sector 10

Bldg 433B, Argonne National Laboratory  
Lemont, IL 60439 (USA)  
Physics Department, Illinois Institute of Technology  
Chicago, IL 60616 (USA)

[d] Prof. J. T. Miller

CSE Division, Argonne National Laboratory  
9700 South Cass Avenue  
Argonne, Illinois 60439-4837 (USA)

Supporting information for this article is available on the WWW under <http://dx.doi.org/10.1002/chem.201300600>.

drogen peroxide (TBHP) as oxidants. In a different study, they also compared the catalytic activity of ceria-supported Au<sub>25</sub> nanorods and nanospheres<sup>[29]</sup> for styrene oxidation and benzalacetone hydrogenation. However, their study was mainly focused on elucidating the effect of calcination on the product yields and a comparison of their activity and selectivity. Tsukuda and co-workers reported that selectivity for styrene epoxide reached 92 % for Au<sub>25</sub> clusters supported on hydroxyapatite when TBHP was used as oxidant.<sup>[25]</sup> In a similar approach, selective oxidation of styrene in the presence of dioxygen by Au<sub>55</sub> clusters was reported by Lambert and co-workers.<sup>[26]</sup> They found a sharp size threshold for activity, with particles larger than 2 nm being completely inactive. Their observations suggest that catalytic activity arises from the altered electronic structure intrinsic to small gold nanoparticles. Further progress has been made by Jiang and co-workers<sup>[30]</sup> by using DFT calculations to show that bare Au<sub>38</sub> (face-centered cubic (fcc) structure) is more catalytically active than Au<sub>55</sub> (fcc structure) for styrene oxidation due to the high electropositive nature of Au atoms on the Au<sub>38</sub> surface.

What is clearly lacking is a concerted effort to correlate the fundamental electronic structure of these atomically precise gold clusters with their catalysis by using a combination of spectroscopic methods, such as X-ray absorption fine structure (XAFS) and ultraviolet photoemission spectroscopy (UPS). Such a correlation is of paramount importance and a first step towards meeting one of the grand science challenges to understand how remarkable catalytic properties emerge from complex correlations of atomic or electronic constituents of the catalysts and how one can control their activity and selectivity.<sup>[31]</sup> We, therefore, not only studied the styrene-oxidation reaction on atomically precise [Au<sub>25</sub>(PPh<sub>3</sub>)<sub>10</sub>(SC<sub>12</sub>H<sub>25</sub>)<sub>5</sub>Cl<sub>2</sub>]<sup>2+</sup> (Au<sub>25</sub>-*bi*) and [Au<sub>25</sub>-(SCH<sub>2</sub>CH<sub>2</sub>Ph)<sub>18</sub>]<sup>-</sup> (Au<sub>25</sub>-*i*) catalysts, but also made an effort to understand the electronic structure of the catalysts by using a combination of synchrotron radiation-based XAFS and UPS, an approach rarely used previously.<sup>[32–34]</sup> XAFS (including X-ray absorption near edge structure (XANES) and extended X-ray absorption fine structure (EXAFS)) is a powerful tool to explore the local atomic and electronic structure of different kinds of gold nanoclusters.<sup>[20,35–46]</sup> The UPS is particularly sensitive in the surface region (ca. 1 nm), providing information about the valence-band structure near the Fermi level, which has been employed to investigate bare Au, as well as ligand-stabilized Au nanoparticles.<sup>[47–50]</sup> Our own recent investigation utilizing UPS confirms s–d hybridization in partially “exposed” Au<sub>38</sub>(SR)<sub>24</sub> clusters deposited on the native SiO<sub>2</sub> oxide in addition to pointing towards the importance of ligand effect.<sup>[50]</sup> Our hypothesis was that a combination of these two techniques enables us to more completely understand the relationship between the local atomic environment, electronic structure and catalytic selectivity and activity of Au<sub>25</sub>-*bi* and Au<sub>25</sub>-*i* nanoclusters.

## Results and Discussion

The UV/Vis absorption spectra obtained for both Au<sub>25</sub>-*i* and Au<sub>25</sub>-*bi* clusters are in agreement with the literature (Figure S1 in the Supporting Information).<sup>[51,52]</sup> The spectrum for Au<sub>25</sub>-*bi* clusters shows discrete peaks typical of molecule-like electronic levels, whereas the spectrum for the Au<sub>25</sub>-*i* clusters shows broad absorption bands at  $\lambda = 400, 450,$  and 670 nm. The matrix-assisted laser-desorption ionization (MALDI) of the clusters was also obtained to ascertain their size (Figure S2 in the Supporting Information). To investigate the catalytic activity of clusters, the as-prepared Au<sub>25</sub>-*bi* and Au<sub>25</sub>-*i* clusters were separately immobilized onto silica supports (fumed silica) by using conventional wet impregnation method and were utilized as catalysts for oxidation of styrene. The catalysis reaction was performed using uncalcined cluster samples to ensure comparison of the results was made on clusters of the same size. The styrene-oxidation procedure was modified from previously reported work by Jin and co-workers.<sup>[24]</sup> The oxidation reaction was carried out by using acetonitrile as a solvent and TBHP as oxidant for both the clusters. Prior to performing the oxidation, a blank reaction without the catalyst was carried out to confirm that the catalytic activity was solely due to the clusters. Thermogravimetric analysis (TGA) was also performed on the catalyst samples before and after the catalysis reaction to ensure there is no leaching of the ligands during the process. The TGA results showed nearly equal weight loss for the catalyst samples before and after reaction confirming that the ligands were intact during the catalysis reaction (Figure S3 in the Supporting Information). The oxidation of styrene catalyzed by Au<sub>25</sub>-*i* resulted in 66 % overall conversion with decrease in selectivity from benzaldehyde (48 %) to styrene oxide (46 %), and benzene acetaldehyde (6 %). However, the catalysis of styrene by using Au<sub>25</sub>-*bi* led to decreased conversion (43 %) albeit with higher selectivity for benzaldehyde formation (75 %) compared to styrene oxide (16 %) and benzene acetaldehyde (8 %).

The normalized Au L<sub>3</sub>-edge XANES spectra of Au<sub>25</sub>-*bi* and Au<sub>25</sub>-*i* clusters along with Au foil are shown in Figure 1. The features in the Au<sub>25</sub>-*bi* and Au<sub>25</sub>-*i* spectra, including resonance peak position and shape, were similar to the bulk gold foil. It indicates that the local environment of Au is still similar to bulk gold. The oscillations beyond the absorption edge in Au<sub>25</sub>-*bi* and Au<sub>25</sub>-*i* XANES spectra were broadened, which were related to lower coordination number, higher structural disorder, and change of bonding distance in comparison with the bulk gold foil, which is typical for nanoclusters. The small shift in absorption-edge energy  $E_0$  in Au<sub>25</sub>-*bi* (0.7 eV) and Au-*i* (0.4 eV) relative to the Au foil was consistent with the observation of d-electron depletion. It also suggests that the Au<sub>25</sub>-*i* and Au<sub>25</sub>-*bi* clusters were mostly in metallic Au<sup>0</sup> state and possibly partially oxidized Au<sup>I</sup>. There is an increase of intensity of the shoulder near the absorption edge (white line) was observed in Au<sub>25</sub>-*bi* and Au<sub>25</sub>-*i* spectra relative to the bulk Au. The white line intensity of Au L<sub>3</sub>-edge is associated with 2p<sub>3/2</sub> to 5d transition.

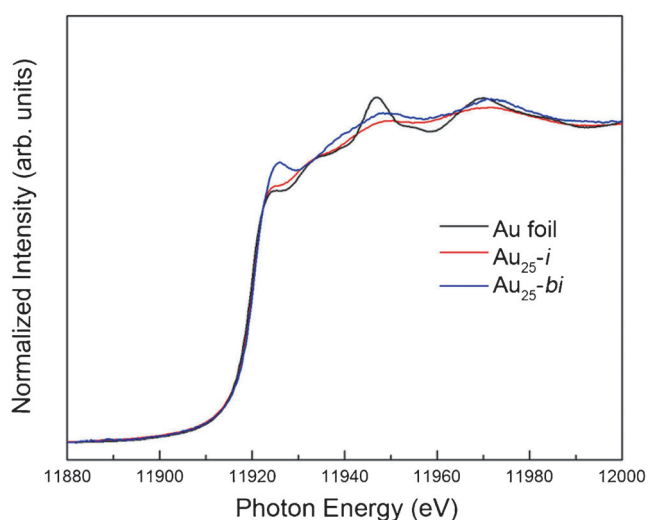


Figure 1. Normalized Au L<sub>3</sub>-edge XANES spectra of Au<sub>25</sub>-bi, Au<sub>25</sub>-i clusters, and gold foil.

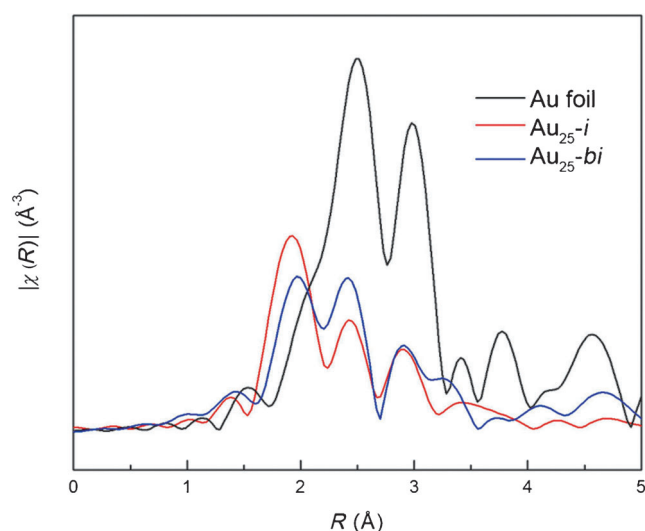


Figure 2. Fourier transformed EXAFS data ( $k^2$  weighting,  $k$  range: 2–11.5 Å<sup>-1</sup>) of Au<sub>25</sub>-i, Au<sub>25</sub>-bi clusters, and gold foil.

The intensity of the first resonance in Au L<sub>3</sub>-edge XANES is usually used to evaluate the unoccupied d-band states of Au clusters.<sup>[39,41,53]</sup> The white line of bulk Au is contributed by s–p–d hybridization.<sup>[44,54,55]</sup> For bare Au and polymer-stabilized Au nanoclusters,<sup>[20,44–46]</sup> the d–d interaction is very strong and s–d hybridization is relatively weak. Thus, the corresponding white line intensity is lower than bulk Au. These observations have been previously attributed to the strong ligand effect on small gold nanoclusters.<sup>[39,41]</sup> The white line of Au<sub>25</sub>-bi spectra was larger than that of Au<sub>25</sub>-i, which in turn was slightly larger than bulk Au. It suggests the number of unoccupied d-band states of Au<sub>25</sub>-bi is larger than that of Au<sub>25</sub>-i, which is in turn larger than bulk Au.

The Fourier transform of Au L<sub>3</sub>-edge EXAFS with  $k^2$  weight is presented in Figure 2. The radial positions of peaks represent the average distance between the Au atom and its near neighbors within 5 Å. The fitting results for Au<sub>25</sub>-bi and Au<sub>25</sub>-i are shown in the Table 1 (fitted data of the Au L<sub>3</sub>-edge  $k^2$ -weighted of EXAFS  $\chi(k)$  spectra shown in Figure S4 in the Supporting Information). The first prominent peak at approximately 2.3 Å in both Au<sub>25</sub>-bi and Au<sub>25</sub>-i nanoclusters was absent in the Au foil, which confirmed S(P) bonding to Au atoms leading to the change in the local environment of the Au clusters. The nearest neighbor at 2.3 Å in Au<sub>25</sub>-i was contributed by Au–S single scattering. For Au<sub>25</sub>-bi, the peak at 2.3 Å was likely associated with

Au–S(P) single scattering, because the contributions from Au–S and Au–P scattering were indistinguishable. The high Au–S(P) coordination numbers in samples, especially for Au<sub>25</sub>-i, indicated the presence of sulfur and/or phosphorous. The first Au–Au single scattering in Au foil was at 2.88 Å.<sup>[29,56]</sup> It was 2.80 Å for Au<sub>25</sub>-i and 2.82 Å for Au<sub>25</sub>-bi, 0.08 and 0.06 Å shorter than that in Au foil, respectively, which was consistent with the previous observations.<sup>[36,38,42]</sup> The first-shell Au–Au bonding distance was reported at 2.78 Å in thiolate-protected Au<sub>38</sub><sup>[2]</sup> at 2.80 Å in Au<sub>55</sub>-(PPh<sub>3</sub>)<sub>12</sub>Cl<sub>6</sub><sup>[40,43]</sup> and at 2.83 Å in Au<sub>144</sub>(SR)<sub>60</sub>.<sup>[41]</sup> The amplitude of the first-shell Au–Au in Au<sub>25</sub>-bi and Au<sub>25</sub>-i was much smaller than that in bulk Au, implying the low coordination numbers and higher structural disorder present in small Au particles. The first-shell Au–Au coordination number for Au<sub>25</sub>-bi is 6.9, which is similar to the experimental result and the calculated value for the previously assigned Au<sub>13</sub> cluster in icosahedron structure.<sup>[38,42]</sup> It is in agreement with our proposal of the molecular structure of biicosahedral Au<sub>25</sub> cluster: two icosahedral Au<sub>13</sub> cages adjoined through one sharing Au atom and the Au<sub>25</sub> core, stabilized by phosphorous and sulfur ligands. This value is also very close to the 1–2 nm gold particles.<sup>[21,57]</sup> The coordination number of the first Au–Au shell in Au<sub>25</sub>-i is 4.8, which is much smaller than in the case of Au<sub>25</sub>-bi. It is likely to be due to differences in the local atomic structures of the two Au<sub>25</sub> clusters, as the

average Au–Au coordination number is sensitive to the local atomic arrangement of the clusters.<sup>[38,58]</sup> The presence of -S-Au-S-Au-S- staples on the Au<sub>13</sub> core in the Au<sub>25</sub>-i cluster results in decreasing first shell Au–Au coordination number and increasing Au–S coordination number at the same time.<sup>[53,57]</sup>

The ligands significantly affected the electronic structure and local structure of the Au<sub>25</sub>-bi and Au<sub>25</sub>-i nanoclusters. The XANES study at the K-edges of sulfur and phosphorous was another way

Table 1. EXAFS fit results of Au<sub>25</sub>-bi and Au<sub>25</sub>-i clusters.

Sample	1st shell Au–Au bond length [Å]	1st shell coordination number (Au)	Au–S(P) bond length [Å]	Coordination number (S/P)	d-Band depletion (relative)	Binding energy (relative)
Au <sub>25</sub> -bi	2.82 ± 0.03	6.9 ± 1.3	2.30 ± 0.05	0.7 ± 0.4	high	high
Au <sub>25</sub> -i	2.80 ± 0.04	4.8 ± 1.3	2.30 ± 0.04	1.2 ± 0.4	low	low
Au <sub>38</sub>	2.78 <sup>2</sup>	2.5 <sup>2</sup>	2.30 <sup>2</sup>	1.1 <sup>2</sup>	lower	lower

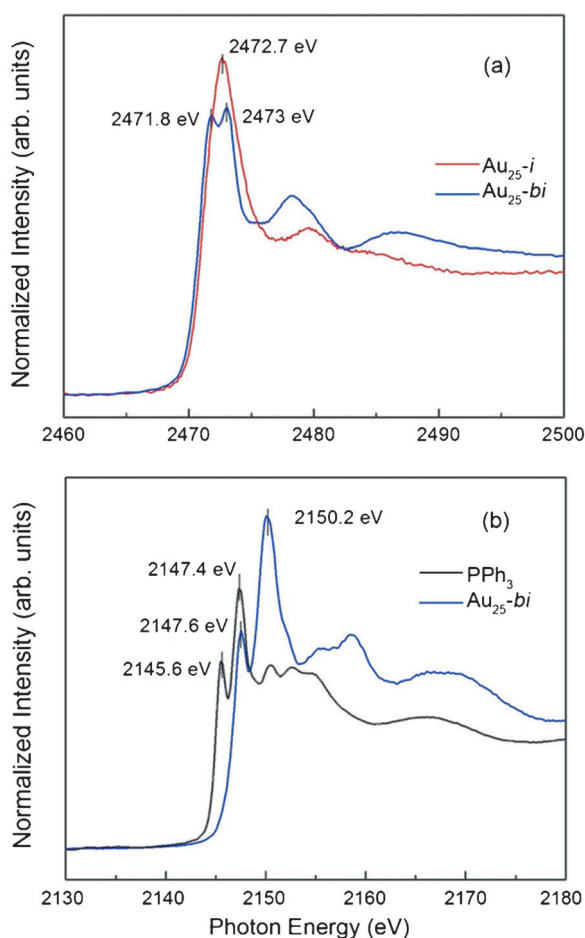


Figure 3. a) Normalized sulfur K-edge XANES spectra of  $Au_{25-bi}$  and  $Au_{25-i}$  clusters; b) normalized phosphorous K-edge XANES  $Au_{25-bi}$  and  $PPh_3$ .

to probe the Au-ligand interaction from the perspective of S and P. As seen in Figure 3 a, the normalized sulfur K-edge XANES spectra of  $Au_{25-bi}$  and  $Au_{25-i}$  showed different features. The white line in  $Au_{25-i}$  XANES at 2472.7 eV was assigned to S 1s to S–C transition.<sup>[41]</sup> The white line splitting in the  $Au_{25-bi}$  cluster spectrum was observed at 2471.8 and 2473 eV. It was probably the result of differences in Au–S bonds in  $Au_{25-bi}$  and  $Au_{25-i}$  clusters because the XANES is quite sensitive to the chemical environment of the absorbing atom. The  $Au_{25-bi}$  contained both sulfur and phosphine ligands, so the phosphorus K-edge XANES of  $Au_{25-bi}$  (Figure 3 b) was collected along with that of  $PPh_3$ , as a reference. The first strong shift in resonance to 2147.4 and 2150.2 eV by 1.8 and 2.6 eV in comparison to  $PPh_3$  was due to the bonding between Au and phosphine li-

gands. By considering the Au  $L_3$ -edge XANES results and difference in electronegativity between P and Au, it is reasonable to assume that electrons are transferred from Au to P. Similar result has been reported on mixed ligand stabilized  $Au_{13}$  clusters.<sup>[42]</sup> The charge transfer from Au to P in  $Au_{13}(PH_3)_6$  clusters was also previously supported by the DFT analysis.<sup>[59]</sup>

Upon calcination of the catalysts, there was a distinct change observed in their catalytic activity. The calcined  $Au_{25-i}$  clusters showed a better conversion of 77% with selectivity of benzaldehyde (70%), styrene oxide (22%), benzene acetaldehyde (3%), and acetophenone (5%), whereas the calcined  $Au_{25-bi}$  clusters had a conversion of 67% with selectivity of the products being benzaldehyde (47%) and styrene oxide (53%). These catalysis results are in agreement with those earlier published by Jin et al.,<sup>[24]</sup> wherein a 6–10% increase in catalytic activity was observed for calcined samples over uncalcined samples (Table 2).

There is a clear effect of calcination on the catalytic activity and product selectivity of the catalysts. Although the uncalcined  $Au_{25-i}$  sample showed almost equal selectivity towards benzaldehyde and styrene oxide, the calcined sample favored the formation of benzaldehyde over styrene oxide. Conversely, for  $Au_{25-bi}$  clusters, the uncalcined sample favored the formation of benzaldehyde over styrene oxide, whereas the calcined sample showed comparable selectivity for both. Not surprisingly, in either case, the calcined samples showed higher catalytic activity (conversion percentage) than the uncalcined samples. The increased catalytic activity of the calcined samples can be attributed to the increased accessibility of the catalyst surface due to partial removal of ligands. The nature of the oxidant also played a significant role in determining the selectivity of the products. For example, TBHP is known to be activated even on larger particles,<sup>[17,24]</sup> and hence, the observed selectivity for calcined samples was different from the uncalcined samples.

Taking  $Au_{25-i}$  as an example, Au  $L_3$ -edge EXAFS was performed on silica supported  $Au_{25-i}$  nanoclusters after calcination at 200°C for 2 h in vacuum. After calcination treatment, the Au–S scattering and Au–low Z-scattering contribution in  $Au_{25-i}$  was negligible, because the thiolate ligands were mostly removed. The first shell Au–Au coordination

Table 2. Catalytic-activity comparison for uncalcined and calcined  $Au_{25-bi}$  and  $Au_{25-i}$  clusters.

Reaction conditions	Selectivity for different products [%]				Total conversion [%]
	Benzaldehyde	Styrene oxide	Benzene acetaldehyde	Acetophenone	
Styrene, TBHP, acetonitrile, 75 °C, $Au_{25-i}@SiO_2$ (uncalcined)	48	46	6	–	66
Styrene, TBHP, acetonitrile, 75 °C, $Au_{25-bi}@SiO_2$ (uncalcined)	75	16	8	–	43
Styrene, TBHP, acetonitrile, 75 °C, $Au_{25-i}@SiO_2$ (calcined)	70	22	3	5	77
Styrene, TBHP, acetonitrile, 75 °C, $Au_{25-bi}@SiO_2$ (calcined)	47	53	–	–	67

Table 3. EXAFS fit results of Au<sub>25</sub>-i/SiO<sub>2</sub> clusters calcined in the air and He.

Sample	Paths	Bond length $R$ [Å]	Coordination number	Debye–Waller factor [Å <sup>-1</sup> ]	Energy shift $\Delta E$ [eV]
Air 100 °C	Au–Au	2.84 ± 0.02	4.9 ± 0.9	0.014	5.3 ± 1.9
	Au–S	2.28 ± 0.02	1.5 ± 0.2	0.008	
Air 200 °C	Au–Au	2.83 ± 0.01	9.7 ± 1.2	0.013	3.0 ± 0.7
	Au–S	2.25 ± 0.04	0.4 ± 0.2	0.009	
Air 300 °C	Au–Au	2.83 ± 0.01	10.8 ± 0.7	0.015	2.8 ± 0.9
He 100 °C	Au–Au	2.83 ± 0.01	6.4 ± 1.5	0.014	4.2 ± 1.1
	Au–S	2.29 ± 0.01	1.2 ± 0.3	0.008	
He 200 °C	Au–Au	2.82 ± 0.01	8.6 ± 1.4	0.014	2.5 ± 0.9
	Au–S	2.24 ± 0.02	0.5 ± 0.2	0.009	
He 300 °C	Au–Au	2.82 ± 0.02	9.2 ± 1.1	0.015	2.3 ± 1.5
	Au–S	2.22 ± 0.05	0.2 ± 0.1	0.003	

number increased to about 9.5 in calcined Au<sub>25</sub>-i/SiO<sub>2</sub>, which slightly changed to 8.5 after catalysis (Table S1 in the Supporting Information). The increase of the first shell Au–Au coordination number indicated the growth of Au particle size on SiO<sub>2</sub>, which was not surprising, based on previously published results, after thermal treatment of ligand protected Au nanoclusters.<sup>[24,60]</sup>

The electronic and geometric changes in silica-supported Au<sub>25</sub>-i nanoclusters during the calcination in air and helium (He) was probed using in situ XANES and EXAFS at Au L<sub>3</sub>-edge to understand how the local environment of the atomically precise Au catalyst changes during the calcination treatment. The white line intensity in XANES spectrum of Au<sub>25</sub>-i/SiO<sub>2</sub> calcined at 300 °C was smaller than that of the bulk Au, which was associated with the d-band electron counts suggesting that the calcination treatment at 300 °C removed most of the ligands, and thus the quantum size effect dominated d-band electron character (Figure S5a in the Supporting Information). It is similar to the case of bare Au clusters.<sup>[21,44]</sup> The fitting results of Au L<sub>3</sub>-edge EXAFS are summarized in Table 3. It was found that the first shell Au–Au bond remained at about 2.83 Å, whereas the coordination number increased with the increase in temperature. The significant change of coordination number happened around 200 °C, especially for sulfur. Air appeared to be more effective in assisting the removal of the ligands than He gas at the same temperature. At 300 °C, the  $k^2$ -weighted EXAFS  $\chi(k)$  of Au<sub>25</sub>-i clusters with fewer ligands still showed higher disorder and low coordination number relative to bulk Au (Figure S5b in the Supporting Information). The average particle size of the Au<sub>25</sub>-i/SiO<sub>2</sub> after calcination to 300 °C was approximately 3–4 nm.<sup>[20]</sup>

The UPS was employed to study the surface electronic structure of ligand-stabilized Au<sub>25</sub>-bi and Au<sub>25</sub>-i clusters, particularly how chemical nature of ligands and size effect can be correlated with their electronic structure. The valence-band spectra of gold clusters gave the characteristics of the 6s and 5d bands density of states. In a previous study of thiolate-stabilized Au<sub>38</sub> nanoclusters supported on Si(111) wafer, it was shown that the valence-band spectra of Au<sub>38</sub> barely resembled the gold-valence band features before sputtering.<sup>[50]</sup> The intensity of 5d-band features at about 3 and 6 eV starts to increase after gentle Ar sputtering

cycle and began to be more pronounced at about 3.4 eV for 5d<sub>5/2</sub> orbital.<sup>[50]</sup> As can be seen in Figure 4a, the valence-band photoemission experiments of Au<sub>25</sub>-bi and Au<sub>25</sub>-i nanoclusters revealed higher binding energies for gold d-band center ( $E_d$ ) of Au<sub>25</sub> clusters (Au<sub>25</sub>-bi (4.56 eV), Au<sub>25</sub>-i (4.36 eV)) relative to bulk Au (4.25 eV). The d-band center of Au<sub>25</sub>-bi and Au<sub>25</sub>-i clusters with a higher binding energy

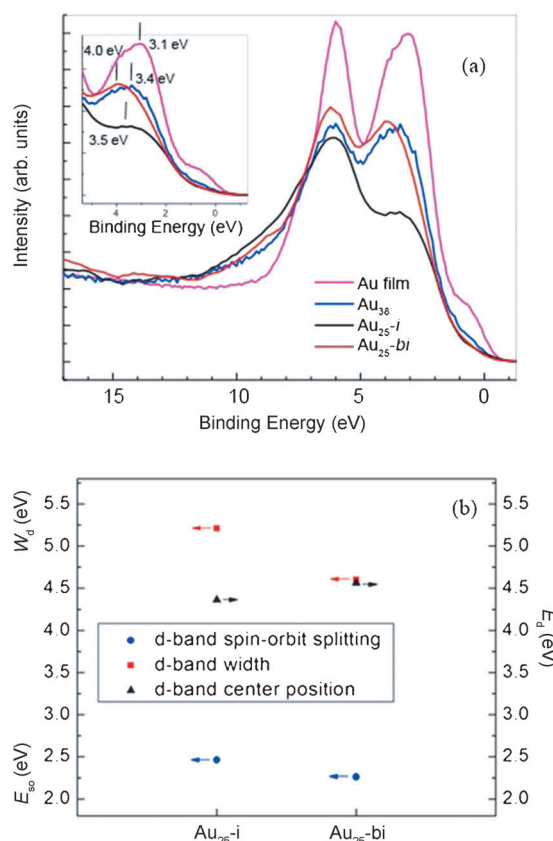


Figure 4. Valence-band photoemission spectra of Au<sub>25</sub>-bi (red), Au<sub>25</sub>-i (black; without sputtering), and Au<sub>38</sub> clusters (blue; after sputtering to remove the thiolate ligands) deposited from solution on SiO<sub>2</sub> native oxide surfaces prepared on Si(111), compared to a micron thick (111) textured gold film (magenta). All spectra were taken at a photon energy of 84 eV; b) d-band width ( $W_d$ ), d-band apparent spin–orbit splitting ( $E_{so}$ ) and d-band center position ( $E_d$ ) of Au<sub>25</sub>-bi and Au<sub>25</sub>-i nanoclusters obtained from (a). The region close to Fermi level is shown as an inset.

may be due to the presence of partially oxidized Au atoms in them, an observation also supported by the analysis of XANES spectra. The d-band width ( $W_d$ ) and apparent spin-orbit splitting ( $E_{so}$ ) were narrower in smaller size nanoclusters ( $Au_{25-bi} < Au_{25-i} < Au_{38} < \text{bulk Au}$ ). This behavior was also seen previously from valence-band spectra studies on thiolate-capped Au clusters,<sup>[29,41]</sup> as well as the observations on bare Au nanoclusters (fcc structure) to some extent.<sup>[47,48]</sup> Both valence-band spectra for  $Au_{25-bi}$  and  $Au_{25-i}$  (synchrotron-radiation flux normalization was done during comparison of photoemission intensities; see Figure 4) were collected without any sample treatment. It means that any difference in the intensity of the experimental bands can be attributed to chemical nature of ligand assuming different bond strengths or just simple presence/absence of ligands on the surface of the clusters. The intensity of 5d band for  $Au_{25-bi}$  was slightly higher than  $Au_{25-i}$  clusters, implying that the contribution from surface Au atoms in  $Au_{25-bi}$  is higher than for  $Au_{25-i}$ . Another possible reason for such electronic structure difference may be simply different net charges on  $Au_{25-bi}$  and  $Au_{25-i}$  (positive vs. negative). The suppression of the intensity of 5d<sub>5/2</sub> band in  $Au_{25-i}$  spectrum may imply that charge transfer from Au d band to sulfur is mainly contributed by d<sub>5/2</sub> electrons in  $Au_{25-i}$  nanoclusters. Such change in electronic structure relative to  $Au_{25-bi}$  could be related to the different local structure of  $Au_{25-i}$ , for example, the presence of -S-Au-S-Au-S- staples. A close look at the spectra indicated higher 6s-band density of states at the Fermi level region for  $Au_{38}$  cluster than  $Au_{25-bi}$  and  $Au_{25-i}$  nanoclusters. Despite the fact that the photoemission intensity in that region was quite lower than that for the gold film, it still suggested that  $Au_{38}$  could be considered as more metallic than  $Au_{25-bi}$  and  $Au_{25-i}$  in accordance with the observed trend for d-band binding energies.

The differences seen in the intensity of gold d band in the valence-band spectra for  $Au_{25-bi}$  and  $Au_{25-i}$  while using photon energies in the range of 60–80 eV almost vanished, although photon energy was increased to over 100 eV (as shown in Figure 5 spectra recorded at 125 eV). In spite of close similarities in valence band at this photon energy, an enhanced intensity of gold 4f band (at about 84 and 88 eV with respect to the Fermi level) for  $Au_{25-bi}$  clusters was clearly seen, whereas it was barely visible for  $Au_{25-i}$ . This re-

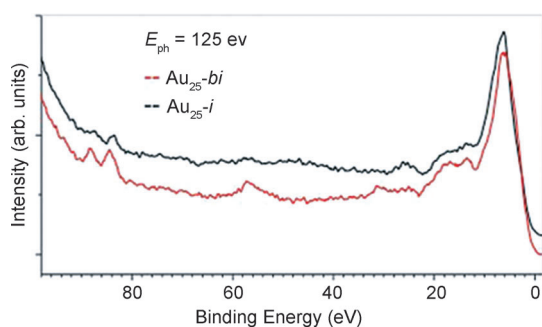


Figure 5. Wide-range ultraviolet photoemission spectra of ligand-stabilized  $Au_{25-bi}$  and  $Au_{25-i}$  nanoclusters recorded at 125 eV photon energy at room temperature.

flects that the contribution from the surface Au atoms in  $Au_{25-bi}$  was larger than that in  $Au_{25-i}$ . One of the reasonable explanations seems to be the easier removal of ligands in  $Au_{25-bi}$  clusters compared to thiol ligands in staple motif layer of  $Au_{25-i}$  under ultrahigh vacuum (UHV) condition. This is consistent with the hypothesis that the phosphine ligands in  $Au_{25-bi}$  are more weakly bound to the Au clusters than the thiol ligands in  $Au_{25-i}$ , which was also seen in our previous investigations on  $Au_{38}$ .<sup>[50]</sup> The observed correlation was consistent with the increasing d-band intensity, although thiol ligands in  $Au_{38}$  were removed after Ar sputtering cycle.<sup>[50]</sup> The 4f band for  $Au_{25-bi}$  showed a positive shift relative to  $Au_{25-i}$ , which was consistent with the observation of d-band shift.

The correlation between the catalytic activity and electronic structure of bare Au catalysts shows that differences in CO oxidation activity of Au clusters can be explained by the change in the s-p-d hybridization and increased d-electron density in smaller particles.<sup>[21]</sup> The more negatively charged Au core in polymer-stabilized Au clusters was more active in aerobic oxidation of alcohols, because  $O_2$  is more readily activated by the higher negative charge on the Au core to promote the oxidation reaction. Furthermore, with Ag doping (<10%), the catalytic activity of the polymer-stabilized Au clusters was enhanced due to the anionic charge transferred from Ag to Au sites.<sup>[46]</sup>

The XAFS and UPS results in the present study revealed differences in the d-band structure of the  $Au_{25-bi}$  and  $Au_{25-i}$  clusters. Higher d-band depletion of Au sites in  $Au_{25-bi}$  in comparison with the  $Au_{25-i}$  clusters, due to more d-band electron transferred to ligands, is likely to make the Au sites in  $Au_{25-bi}$  clusters more relatively electropositive (Table 1). This could be correlated to their activity and selectivity for the styrene oxidation reaction, in which the uncalcined  $Au_{25-bi}$  clusters favored the formation of more oxidized product benzaldehyde over styrene oxide. For uncalcined samples containing ligands, the interaction between the Au core and TBHP is weak. Thus, selectivity is mainly determined by the charge of Au core. However, for the calcined samples the interaction between the Au clusters and oxidant TBHP has to be considered. The calcined  $Au_{25-i}/SiO_2$  displayed higher selectivity to benzaldehyde than uncalcined  $Au_{25-i}/SiO_2$ , though the Au core became more electronegative after calcination. The hybridization between TBHP molecular states and Au d-band states in calcined  $Au_{25-i}/SiO_2$  interaction may be responsible for promoting the formation of benzaldehyde in styrene oxidation.

The styrene oxidation can be understood to proceed in different pathways on each of these two types of uncalcined Au clusters. Uncalcined  $Au_{25-i}$  produced benzaldehyde and styrene oxide as the major products at comparable selectivities, whereas uncalcined  $Au_{25-bi}$  was more selective to benzaldehyde than styrene oxide. We propose a styrene-oxidation mechanism that is consistent with that of Jin and co-workers.<sup>[24]</sup> Initially, TBHP is bound to the clusters forming a hydroperoxy species, which later becomes peroxyformate intermediate upon losing a water molecule. The styrene is

likely adsorbing on to this intermediate through the C=C activation. The C=C bond interacts with adjacent oxygen atoms on the peroxyformate through  $\pi$ - $\pi$  bonding forming a secondary intermediate that later rearranges to form different product depending on the selectivity of the cluster. Control experiments in the absence of catalyst and also TBHP were carried out to confirm that the catalytic effect was only due to clusters.

## Conclusion

Our results provide an insight into correlation between the local structure, electronic structure, and catalytic selectivity and activity of ligand-stabilized Au<sub>25</sub>-*bi* and Au<sub>25</sub>-*i* nanocluster catalysis. Compared to bulk Au, there is a d-band depletion and Au-Au bond contraction in Au<sub>25</sub>-*bi* and Au<sub>25</sub>-*i* associated with strong ligand binding. The d-band narrowing, apparent spin-orbit splitting reduction, and d-band center shift in ligand-stabilized Au<sub>25</sub>-*bi*, Au<sub>25</sub>-*i* and Au<sub>38</sub> nanoclusters was observed in UPS. The higher electropositivity of uncalcined Au<sub>25</sub>-*bi* compared to Au<sub>25</sub>-*i* could be associated with its higher oxidizing capability leading to enhanced selectivity to benzaldehyde.

On the other hand, calcination led to effective removal of the ligands that resulted in increase in the total conversion of styrene for both Au<sub>25</sub>-*bi* and Au<sub>25</sub>-*i*. However, calcination also led to the increase in the size of Au core and caused the particle size to increase to 4 nm for Au<sub>25</sub>-*i*. The number of d-band hole population decreased compared to the uncalcined Au<sub>25</sub>-*i* clusters, implying decrease in the relative electropositivity after the calcination treatment. Such a decrease in electropositivity still led to increase in selectivity for benzaldehyde; which is in contradiction to the case of catalysis by uncalcined samples. Thus, the electropositivity of Au atoms may not be the dominant factor for catalytic selectivity in calcined Au<sub>25</sub>-*bi*/SiO<sub>2</sub> and Au<sub>25</sub>-*i*/SiO<sub>2</sub> nanoclusters. Instead, the interaction between the catalyst and oxidant TBHP appear to play a key role in the selectivity. While investigations to date attempt to explain nanocluster catalysis based on their electronic and geometric structure,<sup>[68]</sup> our findings point out the importance of atomic purity of catalysts during the catalysis to arrive at meaningful conclusions with respect to correlation of their electronic structure with catalytic properties.

## Acknowledgements

This material is based upon work supported as part of the Center for Atomic Level Catalyst Design, an Energy Frontier Research Center funded by the U.S. Department of Energy, Office of Science, Office of Basic Energy Sciences under Award Number DE-SC0001058. MRCAT operations are supported by the Department of Energy and the MRCAT member institutions. The use of the advanced photon source at ANL was supported by the U.S. Department of Energy, Office of Science, Office of Basic Energy Sciences under Contract No. DE-AC02-06CH11357. Financial support for J.T.M. was provided as part of the Institute for Atom-effi-

cient Chemical Transformations (IACT), an Energy Frontier Research Center funded by the U.S. Department of Energy, Office of Science, Office of Basic Energy Sciences. We are grateful to Dr. Tianpin Wu and Dr. Tomohiro Shibata of MRCAT-10ID beam line for their help during EXAFS measurements of Au L<sub>3</sub>-edge. Acknowledgements are also due to Dr. Vladislav Zyryanov for designing the sample cells used for loading the samples.

- [1] D. Li, C. Wang, D. Tripkovic, S. Sun, N. M. Markovic, V. R. Stamenkovic, *ACS Catal.* **2012**, *2*, 1358–1362.
- [2] S. Gaur, J. T. Miller, D. Stellwagen, A. Sanampudi, C. S. S. R. Kumar, J. Spivey, *Phys. Chem. Chem. Phys.* **2012**, *14*, 1627–1634.
- [3] M. Shekhar, J. Wang, W.-S. Lee, W. D. Williams, S. M. Kim, E. A. Stach, J. T. Miller, W. N. Delgass, F. H. Ribeiro, *J. Am. Chem. Soc.* **2012**, *134*, 4700–4708.
- [4] R. M. Rioux, H. Song, P. Yang, G. A. Somorjai, *Catalysis and Materials Science: The Issue of Size Control* **2008**, 149–166.
- [5] Y. Pérez, M. L. Ruiz-González, J. M. González-Calbet, P. Concepción, M. Boronat, A. Corma, *Catal. Today* **2012**, *180*, 59–67.
- [6] I. Lee, F. Delbecq, R. Morales, M. A. Albitar, F. Zaera, *Nat. Mater.* **2009**, *8*, 132–138.
- [7] M. P. Casaletto, A. Longo, A. Martorana, A. Prestianni, A. M. Venezia, *Surf. Interface Anal.* **2006**, *38*, 215–218.
- [8] E. Gross, J. M. Krier, L. Heinke, G. A. Somorjai, *Top Catal* **2012**, *55*, 13–23.
- [9] Z. J. Li, D. S. Huang, W. Liu, R. M. Xiao, J. Liu, C. Xu, Y. Jiang, L. D. Sun, *Gold Bull.* **2004**, *37*, 3–11.
- [10] C. D. Pina, E. Falletta, M. Rossi, *Chem. Soc. Rev.* **2012**, *41*, 350–369.
- [11] L. Guccia, A. Becka, Z. Pászti, *Catal. Today* **2012**, *181*, 26–32.
- [12] R. Jin, *Nanotechnol. Rev.* **2012**, *1*, 31–56.
- [13] Y. Zhu, R. Jin, Y. Sun, *Catalyst* **2011**, *1*, 3–17.
- [14] J. Hernández, J. Solla-Gullón, E. Herrero, A. Aldaz, J. M. Feliu, *J. Phys. Chem. C* **2007**, *111*, 14078–14083.
- [15] S. H. Brodersen, U. Grønberg, B. Hvolbæk, J. Schiøtz, *J. Catal.* **2011**, *284*, 34–41.
- [16] M. Valden, X. Lai, D. W. Goodman, *Science* **1998**, *281*, 1647–1650.
- [17] A. Sanchez, S. Abbet, U. Heiz, W. D. Schneider, H. Hakkinen, R. N. Barnett, U. Landman, *J. Phys. Chem. A* **1999**, *103*, 9573–9578.
- [18] Y. Zhang, X. Cui, F. Shi, Y. Deng, *Chem. Rev.* **2012**, *112*, 2467–2505.
- [19] T. V. W. Janssens, A. Carlsson, A. Puig-Molina, B. S. Clausen, *J. Catal.* **2006**, *240*, 108–113.
- [20] M. S. Chen, D. W. Goodman, *Catal. Today* **2006**, *111*, 22–33.
- [21] J. T. Miller, A. J. Kropf, Y. Zha, J. R. Regalbutto, L. Delannoy, C. Louis, E. Bus, J. A. van Bokhoven, *J. Catal.* **2006**, *240*, 222–234.
- [22] M. Boronat, A. Corma, *J. Catal.* **2011**, *284*, 138–147.
- [23] R. Jin, *Nanoscale* **2010**, *2*, 343–362.
- [24] Y. Zhu, H. Qian, R. Jin, *Chem. Eur. J.* **2010**, *16*, 11455–11462.
- [25] Y. Liu, H. Tsunoyama, T. Akita, T. Tsukuda, *Chem. Commun.* **2010**, *46*, 550–552.
- [26] M. Turner, V. B. Golovko, O. P. H. Vaughan, P. Abdulkin, A. B. Murcia, M. S. Tikhov, B. F. G. Johnson, R. M. Lambert, *Nature* **2008**, *454*, 981–983.
- [27] Y. Gao, N. Shao, Y. Pei, Z. Chen, X. C. Zeng, *ACS Nano* **2011**, *5*, 7818–7829.
- [28] Y. Zhu, H. Qian, R. Jin, *J. Mater. Chem.* **2011**, *21*, 6793–6799.
- [29] Y. Zhu, H. Qian, A. Das, R. Jin, *Chin. J. Catal.* **2011**, *32*, 1145–1150.
- [30] W. Gao, X. F. Chen, J. C. Li, Q. Jiang, *J. Phys. Chem. C* **2010**, *114*, 1148–1153.
- [31] *Directing Matter and Energy: Five Challenges for Science and the Imagination*, A report from the basic energy sciences advisory committee, DOE, USA **2007**.
- [32] H. Hoffmann, F. Zaera, R. M. Ormerod, R. M. Lambert, J. M. Yao, D. K. Saldin, L. P. Wang, D. W. Bennett, W. T. Tysoc, *Surf. Sci.* **1992**, *268*, 1–10.
- [33] A. K. Chakraborty, K. S. Coleman, V. R. Dhanak, *Nanotechnology* **2009**, *20*, 155704–155709.
- [34] Y. Zheng, D. Qi, N. Chandrasekhar, X. Gao, C. Trodec, A. T. Wee, *Langmuir* **2007**, *23*, 8336–8342.

- [35] C. López-Cartes, T. C. Rojas, R. Litrán, D. Martínez-Martínez, J. M. de La Fuente, S. Penadés, A. Fernández, *J. Phys. Chem. B* **2005**, *109*, 8761–8766.
- [36] M. A. MacDonald, D. M. Chevrier, H. Qian, R. Jin, *J. Phys. Chem. C* **2011**, *115*, 15282–15287.
- [37] D. Zanchet, H. Tolentino, M. C. Martins Alves, O. L. Alves, D. Ugarte, *Chem. Phys. Lett.* **2000**, *323*, 167–172.
- [38] L. D. Menard, S. Gao, H. Xu, R. D. Twisten, A. S. Harper, Y. Song, G. Wang, A. D. Douglas, J. C. Yang, A. I. Frenkel, R. G. Nuzzo, R. W. Murray, *J. Phys. Chem. B* **2006**, *110*, 12874–12883.
- [39] P. Zhang, T. K. Sham, *Phys. Rev. Lett.* **2003**, *90*, 245502–1–245502–4.
- [40] P. D. Cluskey, R. J. Newport, R. E. Benfield, S. J. Gurman, G. Schmid, *Zeitschrift für Physik D: Atoms Molecules and Clusters* **1993**, *26*, 8–11.
- [41] M. A. MacDonald, P. Zhang, H. Qian, R. Jin, *J. Phys. Chem. Lett.* **2010**, *1*, 1821–1825.
- [42] A. I. Frenkel, L. D. Menard, P. Northrup, J. A. Rodriguez, F. Zypman, D. Glasner, S. P. Gao, H. Xu, J. C. Yang, R. G. Nuzzo, *AIP Conf. Proc.* **2007**, *882*, 749–751.
- [43] M. M. Marcus, M. P. Andrews, J. Zegenhagen, A. S. Bommannavar, P. Montano, *Phys. Rev. B* **1990**, *42*, 3312–3316.
- [44] J. A. Van Bokhoven, J. T. Miller, *J. Phys. Chem. C* **2007**, *111*, 9245–9249.
- [45] H. Tsunoyama, N. Ichikuni, H. Sakurai, T. Tsukuda, *J. Am. Chem. Soc.* **2009**, *131*, 7086–7093.
- [46] N. K. Chaki, H. Tsunoyama, Y. Negishi, H. Sakurai, T. Tsukuda, *J. Phys. Chem. C* **2007**, *111*, 4885–4888.
- [47] A. Visikovskiy, H. Matsumoto, K. Mitsuhashi, T. Nakada, T. Akita, Y. Kido, *Phys. Rev. B* **2011**, *83*, 165428–1–165428–9.
- [48] D. C. Lim, I. Lopez-Salido, R. Dietsche, M. Bubeck, Y. D. Kim, *Chem. Phys.* **2006**, *330*, 441–448.
- [49] M. Quinten, I. Sander, P. Steiner, U. Kreibitz, K. Fauth, G. Schmid, *Z. Phys. D* **1991**, *20*, 377–379.
- [50] Y. B. Losovyj, S.-C. Li, N. Lozova, K. Katsiev, D. Stellwagen, U. Diebold, L. Kong, C. S. S. R. Kumar, *J. Phys. Chem. C* **2012**, *116*, 5857–5861.
- [51] Y. Shichibu, Y. Negishi, T. Watanabe, K. N. Chaki, H. Kawaguchi, T. Tsukuda, *J. Phys. Chem. C* **2007**, *111*, 7845–7847 (reference for Au<sub>25</sub>-bi structure adapted in TOC figure).
- [52] M. Zhu, E. Lanni, N. Garg, M. E. Bier, R. Jin, *J. Am. Chem. Soc.* **2008**, *130*, 1138–1139.
- [53] G. Simms, J. D. Padmos, P. Zhang, *J. Chem. Phys.* **2009**, *131*, 214703–1–214703–9.
- [54] L. F. Mattheiss, R. E. Dietz, *Phys. Rev. B* **1980**, *22*, 1663–1676.
- [55] M. G. Mason, *Phys. Rev. B* **1983**, *27*, 748–762.
- [56] *CRC Handbook of Chemistry and Physics*, 75th ed. (Ed.: D. R. Lide), CRC Press, Boca Raton, **1994**.
- [57] M. Zhu, C. M. Aikens, F. J. Hollander, G. C. Schatz, R. Jin, *J. Am. Chem. Soc.* **2008**, *130*, 5883–5885.
- [58] J. Kilmartin, R. Sarip, R. Grau-Crespo, D. Di Tommaso, G. Hogarth, C. Prestipino, G. Sankar, *ACS Catal.* **2012**, *2*, 957–963.
- [59] G. Shafai, S. Hong, M. Bertino, T. S. Rahman, *J. Phys. Chem. C* **2009**, *113*, 12072–12078.
- [60] L. D. Menard, F. Xu, R. G. Nuzzo, J. C. Yang, *J. Catal.* **2006**, *243*, 64–73.
- [61] M. Lemonnier, O. Collet, C. Depautex, J. M. Esteva, D. Raoux, *Nucl. Instrum. Methods Phys. Res. Sect. A* **1978**, *152*, 109–111.
- [62] C. U. Segre, N. E. Leyarovska, L. D. Chapman, W. M. Lavender, P. W. Plag, A. S. King, A. J. Kropf, B. A. Bunker, K. M. Kemner, P. Dutta, R. S. Duran, J. Kaduk, *Synchrotron Radiation Instrumentation: Eleventh U.S. National Conference* (Ed.: P. Pianetta), American Institute of Physics, New York, **2000**, Chapter 512, pp. 419–422.
- [63] M. Newville, *J. Synchrotron. Rad.* **2001**, *8*, 322–324.
- [64] J. J. Rehr, R. C. Albers, *Rev. Mod. Phys.* **2000**, *72*, 621–654.
- [65] B. Ravel, M. Newville, *J. Synchrotron. Rad.* **2005**, *12*, 537–541.
- [66] P. A. Dowben, D. LaGraffe, M. Onellion, *J. Phys. Condens. Matter* **1989**, *1*, 6571–6587.
- [67] M. W. Heaven, A. Dass, P. S. White, K. M. Holt, R. W. Murray, *J. Am. Chem. Soc.* **2008**, *130*, 3754–3755 (reference for Au<sub>25</sub>-i structure adapted in TOC figure).
- [68] H. Li, L. Li, Y. Li, *Nanotech. Rev.* DOI: 10.1515/ntrev-2012-0069.

Received: February 15, 2013

Revised: May 14, 2013

Published online: June 20, 2013